Modulation of Contactless High Intensity Pulsed Electromagnetic Field Induced Electroporation and Gene Delivery Efficacy Using Various Nanoparticles

Abstract

High Intensity Pulsed Electromagnetic Fields (HI-PEMF) can be used to trigger contactless permeabilization of plasma membrane similar to electroporation (EP). The permeabilization efficiency and gene delivery by HI-PEMF *in vitro* is currently inferior to EP. It was suggested that the methodology can be improved with conductive gold nanoparticles (NPs), which are reported to amplify the induced electric field in close proximity with the cell membrane. Therefore, in this work, we have studied different nanoparticles, which varied in material/conductivity (gold, silica), size (10 – 50+ nm), shape (i.e., round and rods), concentration (50 – 200 µg/ml) and functionalization (pegylated or not) and combined them with HI-PEMF (6.7 T x 100 pulses, 1 Hz). The normal CHO and cancer T24 cell lines were used as a model. We have characterized cell membrane permeabilization using propidium iodide and the efficacy of gene delivery using pEGFP-N1. This study shows the potential to increase gene delivery efficacy by combining HI-PEMF treatment with conductive NPs. However, it was concluded that the HI-PEMF induced effects are highly dependent on the cell line, nanoparticle type, concentration and therefore require further investigation.

Keywords: HI-PEMF, membrane permeabilization, gene delivery, nanoparticles

1. Introduction

Gene therapies in general carry the potential to tackle most critical and difficult health issues, including rapid vaccine development like that against SARS-CoV-2 and rare debilitating hereditary diseases [1,2]. Recent successes in clinical studies have further increased interest in gene therapies, but bottlenecks persist including the lack of safe and efficient methods for gene delivery. While viral vectors are a natural choice to deliver nucleic acids into the target cells, their use is limited since they have limited cargo capacity and carry major safety concerns [1,2].

Electroporation is one of the most promising nonviral alternatives, which is based on the application of pulsed electric fields (PEFs) and cell plasma membrane permeabilization. During application of high-intensity PEF (pulses applied via electrodes), the permeability of the cell membrane is increased due to formation of transient hydrophilic pores. At the same time electric pulses facilitates movement of negatively charged nucleic acid by electrophoresis, therefore the transfection method is known as gene electrotransfer (GET) [3]. Success rate of electroporation and GET depend predominantly on pulse parameters, but exact mechanisms of GET are not yet fully elucidated [4]. Gene electrotransfer (GET), i.e. pDNA transfer into cells and gene expression can reach up to 80% success rate in some cells *in vitro* [5]. Electroporation allows introducing also large DNA molecules into cells including CRISPR Cas9, thus enabling gene editing [6]. Electroporation has proven to be extremely useful in biomedical research. It is used in treatment of cancer by facilitating intracellular drug accumulation in cells and thereby increasing its cytotoxicity in a treatment called electrochemotherapy, for gene therapy, DNA vaccination and as a nonthermal soft tissue ablation method [7–9].

Classical electroporation requires electrode contact with a tissue to establish electric field in tissue. Application of high voltage electric pulses via electrodes induces pain and muscle contractions. In case of invasive electrodes, the tissue is damaged, therefore increasing the risk of inflammation. Finally, the mammalian tissues are highly heterogenic, which results in unpredictable spatial electric field distribution [10]. Tissue damage around the electrodes and inability to ensure the required electric field compromises the success of the whole procedure (regions of under or over-treatment). High Intensity Pulsed Electromagnetic Fields (HI-PEMF) is a contactless method, which causes less tissue damage, does not result in pain or muscle contraction but at the same time offers all the benefits of controlled molecular delivery as electroporation does [11,12].

HI-PEMF induced electroporation is based on repetitive pulsed high magnetic fields in the range of a few Teslas. HI-PEMF was shown to increase membrane permeabilization similar to electroporation and can be thus used to increase transmembrane molecular transport [11–14] and introduction of large molecules like plasmid DNA (pDNA) into target cells. HI-PEMF has been also used for successful delivery of siRNA and plasmid encoding GFP protein *in vivo* [15,16] and *in vitro* [17]. Nevertheless, while membrane permeabilization and GET can be achieved using HI-PEMF, its efficacy is inferior when compared to PEF. The improvement of HI-PEMF treatment efficacy is therefore of great interest and one such option represents introduction of nanoparticles (NPs). The interaction between NPs and electromagnetic fields has been demonstrated previously. For example, barium-hexaferrite nanoplatelets were activated by low frequency alternating magnetic fields to disrupt the lipid membrane [18] and gold NPs were shown to be electrophoretically driven close to cell-plasma membrane by pulsed electric fields [19]. Interestingly it has been suggested theoretically and demonstrated experimentally that NPs can facilitate electroporation: GET, drug delivery/electrochemotherapy and even extent of the area of tissue being ablated by irreversible electroporation [20–24]. NPs used in these experiments were mainly carbon nanotubes and conductive/metal NPs like gold and platinum NPs. The underlying assumption is that conductive NPs locally amplify electric field and thus, if close to plasma membrane, allow its electroporation at lower electric fields. It has been shown that the presence of gold NPs can improve the membrane permeabilization efficacy in HI-PEMF treatment [16].

To investigate the influence of nanoparticles properties on HI-PEMF treatment further with the aim to improve membrane permeabilization and gene delivery, we used different nanoparticles, which varied in size, shape, functionalization and material. We determined membrane permeabilization and gene delivery using combination of HI-PEMF treatment and different NPs on different two cell lines *in vitro*.

2. Materials and methods

2.1. Nanoparticles

2.1.1 Chemicals

Hydrogen tetrachloroaurate trihydrate ($HAuCl_4 \cdot 3H_2O$, 99.99%) and sodium hydroxide (NaOH, 98%) were obtained from Alfa Aesar. Silver nitrate (≥99.8%), citric acid monohydrate (99.5–100.5%), bis(p-sulfonatophenyl)phenylphosphine (97%), and L-(+)-ascorbic acid (99.5–100.5%) were purchased from Sigma-Aldrich. Sodium borohydride ($NaBH_4$, 98+%) was supplied by Acros Organics. Sodium chloride (NaCl, ≥99.5%) was obtained from Fisher Scientific. Surfactants and stabilizers including hexadecyltrimethylammonium bromide (CTAB) and Tween 80 were purchased from VWR and Fisher Bioreagents, respectively. O-(2-mercaptoethyl)-O′-methylpolyethylene glycol (PEG, MW 2000) was also obtained from Sigma-Aldrich. All chemicals were used as received, without further purification.

2.1.2 Synthesis and PEGylation of gold nanorods (AuNRs-PEG)

Gold nanorods (AuNRs) were synthesized using a seed-mediated growth method adapted from Nikoobakht and El-Sayed [25]. The synthesis consisted of two main stages: seed preparation and nanorod growth.

Seed preparation: A 5 mL solution of hydrogen tetrachloroaurate(III) trihydrate (0.00050 M) was freshly prepared and cooled prior to use. It was then mixed with 5 mL of 0.2 M CTAB under vigorous stirring. Immediately after, 0.6 mL of ice-cold sodium borohydride (0.010 M) was rapidly added to the mixture. A prompt colour change from yellow to brown indicated the formation of gold seed particles. The mixture was stirred for an additional 2 minutes and subsequently incubated in the dark at 30 °C for 4 hours to allow for seed maturation.

Growth solution preparation and nanorod formation: Prior to growth, all reagents were equilibrated in a water bath at 30 °C for one hour. The following stock solutions were prepared: 127 mL of 0.001 M $HAuCl_4 \cdot 3H_2O$, 127 mL of 0.2 M CTAB, 3.83 mL of 0.0040 M silver nitrate ($AgNO_3$), and 1.786 mL of 0.0788 M L-ascorbic acid. To prepare the growth solution, silver nitrate, CTAB, and the gold precursor were combined under vigorous stirring. The addition of ascorbic acid triggered a rapid colour change from yellow to colourless, indicating the reduction of gold ions to Au^0.

Immediately thereafter, 0.306 mL of the previously prepared seed solution was introduced into the growth mixture, followed by gentle stirring for 30 seconds. The reaction was then left undisturbed to proceed overnight at 30 °C in the dark.

Purification: To remove excess CTAB, the resulting gold nanorods (AuNRs) were purified by two cycles of ultracentrifugation at 20,000 × g for 20 minutes, followed by resuspension in distilled water.

Functionalization with PEG: Gold nanorods were functionalized with polyethylene glycol (PEG) following the method described by Liu *et al*. [26] with slight modifications. Briefly, separate stock solutions were prepared: 2 vol% Tween 80, 25 µL of 0.1 M bis(p-sulfonatophenyl)phenylphosphine (BSSP), 63 µL of 1.6 mM O-(2-mercaptoethyl)-O′-methylpolyethylene glycol (MeO-PEG-SH), and 250 µL of 2 M sodium chloride (NaCl). These compounds were mixed and stirred for 1 minute prior to the addition of the AuNR suspension. The mixture was then gently shaken overnight to allow for complete PEGylation. Following the reaction, the PEG-functionalized gold nanorods (AuNRs-PEG) were purified by two cycles of washing with distilled water to remove excess reagents.

2.1.3 Synthesis of quasi-spherical 10 nm gold nanoparticles (10-AuNPs)

The synthesis of 10 nm gold nanoparticles (10-AuNPs) was adapted from the protocol reported by Ojea-Jiménez et al. [27]. Briefly, 102 mL of 2.45 mM sodium hydroxide and 2.1 mL of 0.34 M sodium citrate were mixed in a round-bottom flask equipped with a reflux condenser and heated in an oil bath until boiling. Once the solution reached boiling temperature, 2 mL of 0.066 M hydrogen tetrachloroaurate trihydrate was rapidly added under vigorous stirring. The solution immediately turned black, followed by a gradual shift to a deep wine-red colour, indicating the formation of gold nanoparticles. Upon completion of the reaction, the colloidal suspension was rapidly cooled to room temperature using an ice bath. The resulting 10-AuNPs were then washed with distilled water to remove residual reagents.

2.1.4 Synthesis of quasi-spherical ~50 nm gold nanoparticles (50-AuNPs)

Gold nanoparticles with an average diameter close to 50 nm were synthesized using a multi-step seed-mediated growth approach, adapted from the method described by Bastús et al. [28]. Stock aqueous solutions of sodium citrate (2.2 mM and 60 mM) and hydrogen tetrachloroaurate (25 mM) were freshly prepared prior to synthesis.

Seed preparation: To produce gold seed particles, 37.5 mL of 2.2 mM sodium citrate solution was heated in a 100 mL round-bottom flask equipped with a reflux condenser and immersed in an oil bath until boiling. Upon reaching the boiling point, 0.25 mL of 25 mM $HAuCl_4$ was rapidly injected under vigorous stirring. A light pink coloration appeared within one minute, indicating the formation of seed nanoparticles. The suspension was then removed from heat and allowed to cool to 90 °C at room temperature.

First growth step: Once cooled, the seed solution was returned to the oil bath and maintained at 90 °C with a reduced stirring speed of 600 rpm. To initiate growth, 0.25 mL of $HAuCl_4$ solution was added to the reaction, followed by two additional 0.25 mL aliquots, each added at 10-minute intervals.

Subsequent growth cycles: In parallel, a secondary growth solution was prepared by heating 13.25 mL of distilled water and 0.5 mL of 60 mM sodium citrate to 90 °C. Once the target temperature was reached, 13.75 mL of the previously prepared nanoparticle suspension was added to this solution. This was followed by three sequential additions of 0.25 mL $HAuCl_4$, each spaced 10 minutes apart. The dilution–growth cycle was repeated four times to incrementally increase particle size.

Purification: Following the final growth step, the resulting gold nanoparticles (50-AuNPs) were washed with distilled water to remove excess citrate and other residual reagents.

2.1.5 PEGylation of gold nanoparticles (10-AuNPs-PEG and 50-AuNPs-PEG)

Both 10 nm and 50 nm gold nanoparticles were functionalized with polyethylene glycol (PEG) using the same protocol. Each nanoparticle suspension was added dropwise into a vigorously stirred solution of 0.125 mM methoxy-terminated PEG-thiol (MeO-PEG-SH) in a total volume of 20 mL. The mixture was allowed to react overnight at room temperature to ensure complete

surface coverage. The following day, PEGylated nanoparticles (10-AuNPs-PEG and 50-AuNPs-PEG) were purified by a single washing step with distilled water to remove unbound PEG molecules.

2.1.6 Synthesis of silica nanoparticles (SiO_2-NPs)

Silica nanoparticles (SiO_2-NPs) were synthesized using a modified Stöber method [29]. In a typical procedure, 50 mL of deionized water, 4.5 mL of aqueous ammonia (NH_3), and 50 mL of a 0.27 M tetraethyl orthosilicate (TEOS) solution were combined in a reaction flask and stirred continuously overnight at room temperature. Upon completion of the synthesis, the resulting silica nanoparticles were collected and purified by three successive washing steps with distilled water.

2.1.7 Characterization of nanoparticles

Transmission electron microscopy (TEM) analysis was performed using a JEOL 2100 microscope equipped with energy-dispersive X-ray spectroscopy (EDXS, JED 2300 EDS). For all nanoparticle types, TEM grids were prepared by drop-casting ~20 microliters of the diluted suspension onto carbon-coated copper grids, followed by air drying at room temperature. Particle size distributions were determined using ImageJ software based on the manual analysis of a statistically significant dataset (N = 500 particles).

Zeta potential measurements were conducted using a Litesizer 500 instrument (Anton Paar, Austria). Nanoparticle suspensions were diluted to a final concentration of 250 µg/mL. Zeta potential measurements were performed in a distilled water (pH was 7.2 – 7.4) as well as in both types of cellular media containing proteins (HAM medium: HAM F-12 growth medium supplemented with 10% fetal bovine serum and DMEM medium: A-DMEM:F12 growth medium supplemented with 5% FBS). using disposable cuvettes for analysis under standard measurement conditions.

2.2. Cells

Chinese hamster ovary cell line (CHO) was purchased from European Collection of Authenticated Cell Cultures. Cells were grown in HAM F-12 growth medium (PAA, Austria) supplemented with 10% fetal bovine serum (FBS, Sigma-Aldrich, USA), L-glutamine (0.5%

for CHO, 2% for H9c2) (StemCell, Canada), penicillin/streptomycin (PAA, Austria) and 0.1% gentamycin (Sigma-Aldrich, USA) in an incubator at 37°C with controlled atmosphere (CHO at 5% CO2, H9c2 at 10% CO2). Human urinary bladder's transitional carcinoma cell line (T24) was purchased from American Type Culture Collection (ATCC). Cells were grown in A-DMEM:F12 growth medium (Gibco, Thermo-Fisher, USA) mixed 1:1 and supplemented with 5% FBS (Gibco) and 4 mM Glutamax (Gibco). Cells T24 were grown in incubator at 37°C with controlled atmosphere (5% CO2).

Growth medium was removed and the trypsin-EDTA (PAA, Austria) was added to detach cells. After 3 minutes fresh medium was added to inactivate trypsin. Cell suspension was then centrifuged at 180 g for 5 minutes, supernatant was removed, cells were resuspended in cells growth media to obtain different concentration of nanoparticles (0,50,100 or 200 μg/ml) and 1 × 10^6 cells/ml or in case of GET 2 × 10^6 cells/ml density. Cell suspension was incubated at 4°C for 15 minutes and afterward HI-PEMF treatment was delivered.

2.3. High Intensity Pulsed Electromagnetic Field (HI-PEMF) treatment

High Intensity Pulsed Electromagnetic Field (HI-PEMF) was applied with pulse generator previously described [13]. As an applicator, solenoid coil was used (11.8 μH), wounded from enamel-insulated copper wire (6 layers × 8 windings, wire diameter: 0.5 mm, and effective radius = 2 mm. The magnetic field was 6.7 T in the middle of the coil, and the induced electric field was up to 20 V/cm near the coil windings, declining towards 0 at the geometric center of the coil. The HI-PEMF was generated using a half-sinusoidal pulse with a peak voltage of 3 kV and a peak electric current of 1 kA [13]. A total of 100 pulses were used delivered at repetition frequency of 1 Hz.

2.4. Permeabilization assay

Prior to HI-PEMF treatment CHO and T24 cells were mixed with propidium iodide (PI, Life Technologies) to a final concentration of 100 μg/ml. Immediately after the treatment 40 μl of cell suspension was transferred to 0.2 PCR tube (ABgene, Thermo Fisher Scientific, Waltham, MA, USA). Three minutes after treatment cell suspension was removed from the PCR tube and the uptake of PI in cells was analyzed by the flow cytometer (Attune NxT; Life Technologies, Carlsbad, CA, USA) using 488 nm blue laser and 574/26 nm band-pass filter. The analysis of

10,000 events was performed by Attune Nxt software. On the dot-plots of forward-scatter and side-scatter the debris and clusters were excluded from the analysis. Fluorescence intensity histograms were used to determine the percentage of PI permeabilized cells. Gating was set according to sham control (0 V, without nanoparticles). Measurements for each data point were repeated three times.

2.5. Gene electrotransfer (GET) assay

Gene electrotransfer was evaluated with plasmid pEGFP-N1 (Clontech Laboratories Inc, Mountain View, CA, USA) encoding green fluorescent protein (GFP) under the control of CMV promotor in the size of 4.7 kb. Plasmid (pDNA) was amplified using Escherichia coli, isolated with HiSpeed Plasmid Maxi Kit (Qiagen, Hilden, Germany) and plasmid concentration was spectrophotometrically determined at 260 nm.

Prior to HI-PEMF treatment CHO cells were mixed with the plasmid to obtain concentration of plasmid at 100 μg/ml. Immediately after the treatment 40 μl of cell suspension with plasmid was transferred to 0.2 PCR tube and after the treatment 10 μl of fetal bovine serum was added to the cells and incubated for another 5 minutes at 37°C. Afterwards cells were diluted in fresh growth medium and the sample was split for two following analysis – percentage of GFP positive cells and viability.

Detection of transfected cells: To determine percentage of GFP positive cells, cells were seeded in growth medium into 24-well plate (Techno Plastic Products AG, Trasadingen, Switzerland) for 24 h at 37 ◦C, 5% CO2. Afterwards cells were harvested and resuspended in 150 μL of phosphate buffer saline (1x PBS) and analyzed using flow cytometer Attune NxT (ThermoFisher Scientific, Waltham, MA, USA) with a blue laser at 488 nm and a 530/30 nm bandpass filter. For every sample 10,000 events were recorded. Fluorescence intensity histograms were used to determine the percentage of GFP positive cells.

Viability: For survival analysis cells were diluted in fresh growth medium and 2×10^4 cells were transferred to 96-well plate (Techno Plastic Products AG, Trasadingen, Switzerland) and incubated at 37°C for 24 hours. According to manufacturer's instructions (CellTiter 96 AQueous One Solution Cell Proliferation Assay, Promega, USA) 20 μl of MTS tetrazolium compound was added to the samples and after 2 hours the absorbance of formazan (reduced

MTS tetrazolium compound) was measured with a spectrofluorometer (Tecan Infinite M200, Tecan, Austria) at 490 nm. The percentage of viable cells was obtained by the normalization of sample absorbance to the absorbance of the control (0 V) with the same nanoparticles type and concentration.

Overall gene electrotransfer was calculated multiplying % of GFP positive cells and survival after GET.

2.6. Statistical analysis

All experiments except for TEM were repeated at least three times. The results are shown as mean ± SD. Statistical analysis was performed using SigmaPlot 11.0 (Systat Software, USA). Statistically significant differences (* $p<0.05$) were determined by one-way ANOVA test and Holm-Sidak post-hoc test.

3. Results

3.1. Characterization of nanoparticles

The effect of nanoparticles on the efficiency of HI-PEMF-induced electroporation was investigated using a variety of conductive gold nanoparticles differing in shape, size, and surface functionalization, as well as non-conductive silica nanoparticles. The physicochemical characteristics of all nanoparticle types are summarized in Table 1. TEM analysis confirmed that the smaller gold nanoparticles (10-AuNPs) exhibited a narrow size distribution, with an average diameter of 12.0 ± 1.1 nm (Figure 1). Dynamic light scattering (DLS) measurements indicated no detectable aggregation upon mixing the nanoparticles with the different media used, yielding mean hydrodynamic sizes of 43.8 ± 0.4 nm, 75.7 ± 3.7 nm, and 78.3 ± 0.8 nm in water, DMEM, and HAM media, respectively (Table 2).

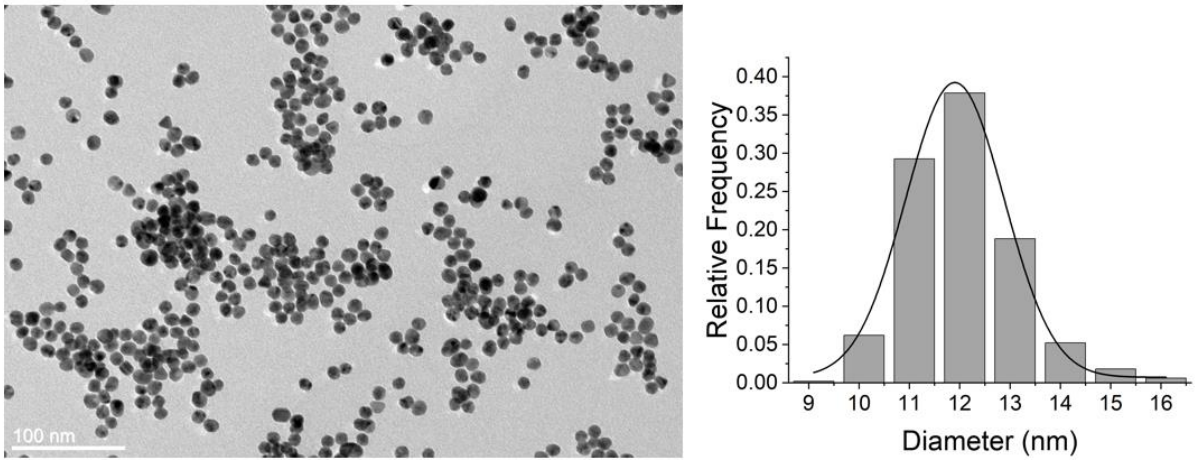

Figure 1. Transmission electron microscopy (TEM) image of 10-AuNPs (left) and corresponding particle size distribution histogram based on TEM analysis (right).

For experimental studies, either citrate-stabilized (carboxyl-terminated surface) or PEG-functionalized (methoxy-terminated surface) gold nanoparticles were used. Zeta potential measurements revealed values of -11.6 ± 0.3 mV for citrate-functionalized and -5.5 ± 1.5 mV for PEG-functionalized nanoparticles (Table 3). These changes in surface potential might affect the interaction of nanoparticles and cell membrane. However, surface charge is likely screened from salts and other components present in the electroporation buffer which reduced the absolute value of zeta potential under experimental conditions. DLS measurements also demonstrated an absence of aggregation of the functionalized nanoparticles in both HAM and DMEM (Table 2).

Table 1. Characteristics of the synthesized nanoparticles used in our study.

Nanoparticles	Material	Shape	Size (nm)*	Surface
50-AuNPs	Gold	Quasi-spherical	57 ± 7	COOH
10-AuNPs	Gold	Quasi-spherical	12 ± 1	COOH
50-AuNPs-PEG	Gold	Quasi-spherical	57 ± 7	PEG
10-AuNPs-PEG	Gold	Quasi-spherical	12 ± 1	PEG
AuNRs-PEG	Gold	Elongated	63 ± 4 length 17 ± 2 diam	PEG
SiO_2-NPs	Silica	Spherical	54 ± 6	-OH

* Size is determined by TEM image analysis.

Table 2: Dynamic light scattering (DLS) characterization of various nanoparticles in water and two different cellular media used.

Nanoparticles	Dispersing solution	Mean hydrodynamic Size (nm)
10-AuNPs	Distilled water	43.8 ± 0.4
10-AuNPs-PEG	Distilled water	52.3 ± 1.1
50-AuNPs	Distilled water	64.1 ± 1.0
50-AuNPs-PEG	Distilled water	75.9 ± 1.9
SiO_2-NPs	Distilled water	104.4 ± 3.7
10-AuNPs	DMEM	75.7 ± 3.7
10-AuNPs-PEG	DMEM	75.5 ± 2.6
50-AuNPs	DMEM	90.4 ± 3.2
50-AuNPs-PEG	DMEM	76.4 ± 0.1
SiO_2-NPs	DMEM	222.3 ± 9.1
10-AuNPs	HAM	78.3 ± 0.8
10-AuNPs-PEG	HAM	85.4 ± 3.7
50-AuNPs	HAM	88.9 ± 3.0
50-AuNPs-PEG	HAM	76.5 ± 2.0
SiO_2-NPs	HAM	491.8 ± 77.5

Table 3. Zeta potential values of various nanoparticles in water and two different cellular media used.

Nanoparticles	Zeta potential value in water	Zeta potential value in HAM	Zeta potential value in DMEM
50-AuNPs	- 41.2 ± 5.7 mV	-9.7 ± 0.5 mV	-10 ± 0.4 mV
10-AuNPs	-15.9 ± 2.2 mV	-11.6 ± 0.3 mV	-11.3 ± 0.2 mV
50-AuNPs-PEG	-41.2 ± 5.7 mV	-3.3 ± 0.7 mV	-2.4 ± 0.2 mV
10-AuNPs-PEG	-23.5 ± 1.7 mV	-5.5 ± 1.5 mV	-6.4 ± 1.3 mV
AuNRs-PEG	-21.6 ± 1.6 mV	-4.2 ± 0.7 mV	-3.6 ± 0.3 mV
SiO_2-NPs	-47 ± 0.6 mV	-10.9 ± 0.6 mV	-0.2 ± 0.1 mV

Larger gold nanoparticles (50-AuNPs) with an average diameter of 56.9 ± 7.0 nm (Figure 2) were also synthesized, featuring the same surface functional groups—carboxyl (citrate-stabilized) or methoxy (PEGylated)—as the smaller particles. Zeta potential measurements indicated values of –9.7 ± 0.5 mV for citrate-functionalized and –3.3 ± 0.7 mV for PEG-functionalized formulations (Table 3). DLS measurements also showed good colloidal stability of both types of nanoparticles in HAM and DMEM media (Table 2).

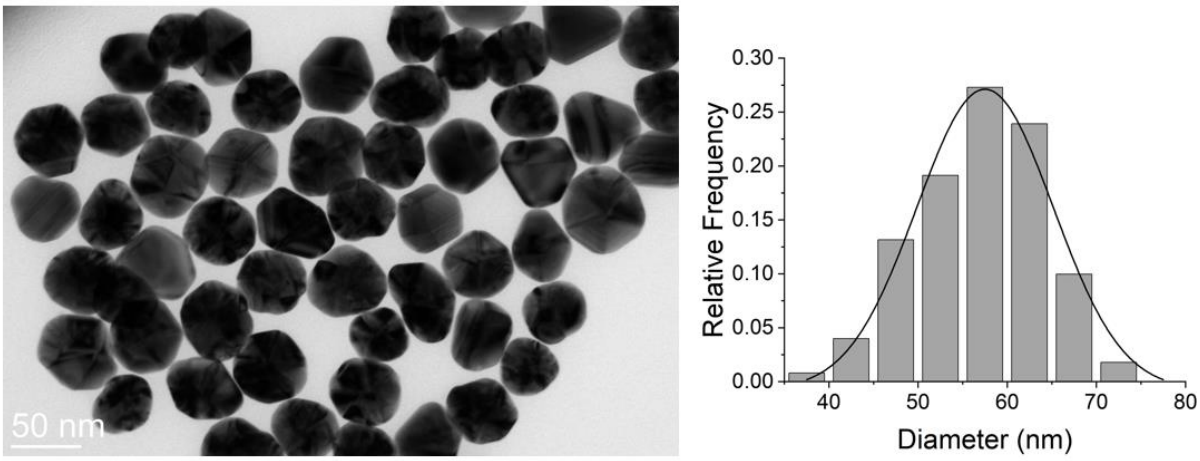

Figure 2. Transmission electron microscopy (TEM) image of 50-AuNPs (left) and corresponding particle size distribution histogram (right), based on TEM analysis.

Gold nanorods were synthesized with an average diameter of 17.1 ± 1.8 nm and length of 63.0 ± 4.4 nm, yielding an aspect ratio of approximately 4.3, to investigate the influence of nanoparticle shape and size. Representative TEM images and corresponding size distribution histograms are shown in Figure 3. The nanorods were synthesized in the presence of cetyltrimethylammonium bromide (CTAB), a surfactant known for its cytotoxicity. To enhance biocompatibility, the CTAB was removed by intense and repeatable washings while remaining traces were replaced with a polyethylene glycol (PEG) coating using a protocol similar to that applied for quasi-spherical nanoparticles. The resulting zeta potential values were comparable to the values measured for the other types of PEGylated nanoparticles included in our study.

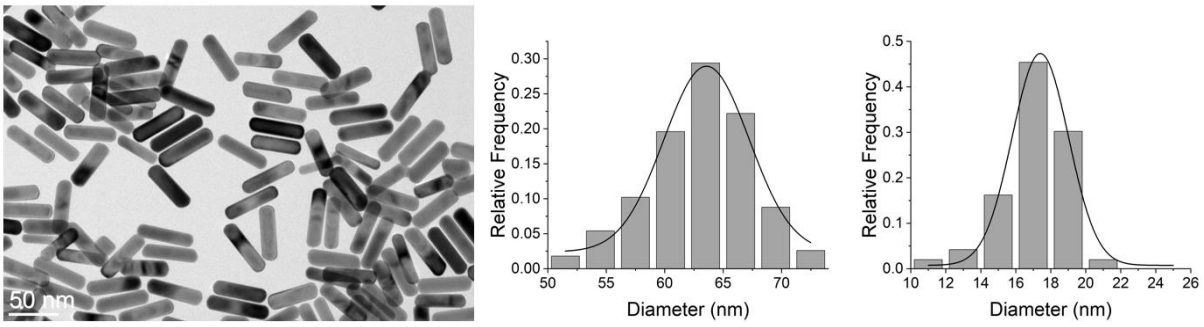

Figure 3. TEM image of gold nanorods (left), with length distribution shown in the center and width distribution on the right.

To evaluate whether the presence of nanoparticles alone affects cells, non-conductive silica nanoparticles (SiO_2-NPs, 53.6 ± 6.1 nm; Figure 4) were synthesized as a control.

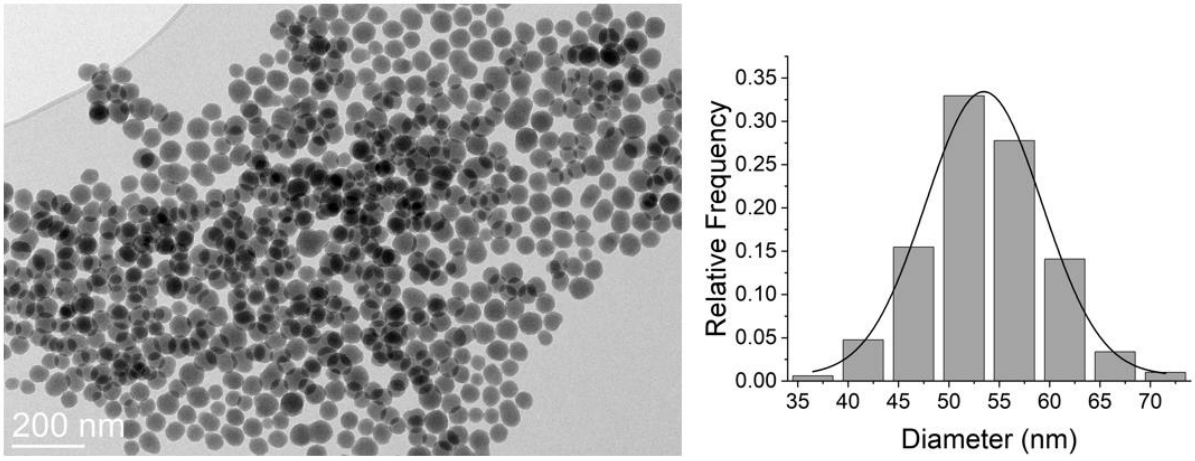

Figure 4. Transmission electron microscopy (TEM) image of spherical silica nanoparticles (left) and corresponding particle size distribution histogram (right), based on TEM analysis.

3.2. Effect of NPs on membrane permeabilization

The influence of NPs (200 μg/ml) was first evaluated on membrane permeabilization efficacy, where intracellular PI accumulation was used as a marker of successfully permeabilized membrane (Figure 5). In the absence of NPs HI-PEMF treatment causes approx. 20% of cell permeability in CHO cells compared to no treatments (control). However, when NPs were added, permeabilization efficacy of HI-PEMF treatment was affected (Figure 5A). When 10-AuNPs and 50-AuNPs were used membrane permeability increased to 25% for 10-AuNPs and 30% for 50-AuNPs, making the permeabilization efficacy higher. Also, while there was a tendency of size dependence (i.e., larger 50-AuNPs caused higher increase in permeability than smaller 10-AuNPs), the differences were not statistically significant ($P < 0.05$).

Interestingly, when the PEG-functionalized gold nanoparticles were used (10-AuNPs-PEG and 50-AuNPs-PEG) the initially positive effects of NPs were reversed - a statistically significant decrease in permeabilization efficacy was triggered (versus HI-PEMF without NPs). Similar trends were observed with different shapes (i.e., rods AuNRs-PEG) or even with different material such as non-conductive control SiO_2-NPs.

To confirm if the observed effects are cell line specific, we have tested T24 cell line in the same context (Figure 5B). Surprisingly, all of the NPs involved in the study triggered the amplification phenomenon and no decrease in permeabilization efficacity was observed, regardless of the NPs type and properties.

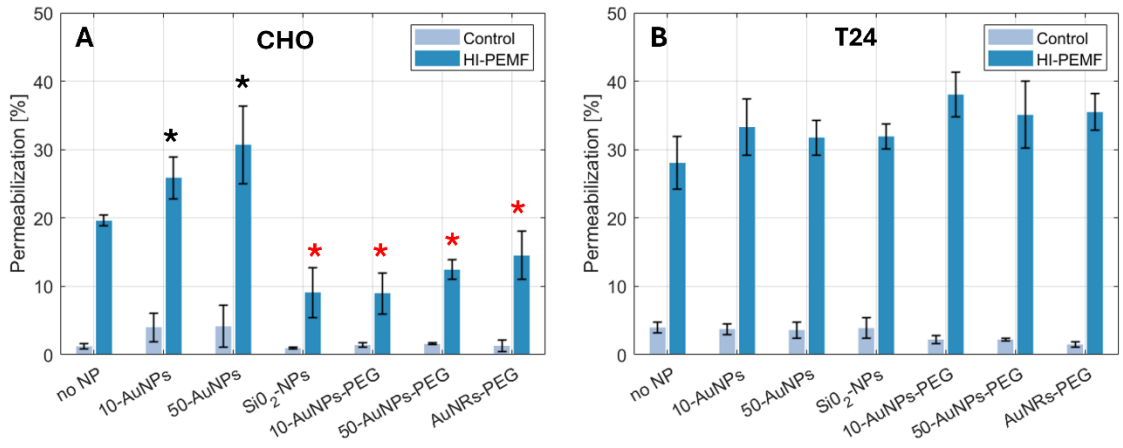

Figure 5. Membrane permeabilization after HI-PEMF treatment on A) CHO and B) T24 cells in the presence of nanoparticles. Results are presented as a mean value and bars represent standard deviation. All HI-PEMF treatments permeabilization was statistically significantly higher with than without HI_PEMF treatment (control). Black asterisk (*) marks a statistically significant increase in HI-PEMF treatment and red asterisk (*) marks a statistically significant decrease in HI-PEMF treatment compared to HI-PEMF treatment without NPs.

3.3. Effect of NPs on gene electrotransfer

As only CHO cell line resulted in increased membrane permeabilization, only CHO cell was used in gene electrotransfer experiments. Since 50-AuNPs caused the highest increase in membrane permeability in CHO cells, the same NPs were used for gene electrotransfer experiments (Figure 6). In addition to the no NPs (0 μg/ml) also 50, 100 and 200 μg/ml of 50-AuNPs were used, to investigate if the effect is NPs concentration dependent. For each concentration of 50-AuNPs in addition to HI-PEMF treatment two controls were used: CTRL1 - control without the plasmid and without the treatment (0V) and CTRL2 - control with the plasmid and without the treatment (0V). This showed that the presence of plasmid or/and nanoparticles by itself, i.e. without the HI-PEMF treatment, was not achieving gene delivery.

When the lowest concentration of NPs (50 μg/ml) was used results showed slight (2.9 %), yet statistically significant ($p<0.05$), increase in gene delivery efficacy compared to HI-PEMF treatment without the presence of NPs. With the increase of NPs concentration there was a declining tendency in gene delivery efficacy. The 50 μg/ml concentration was optimal within the studied range of concentrations. It should be noted that none of the treatments used in the study affected cell viability.

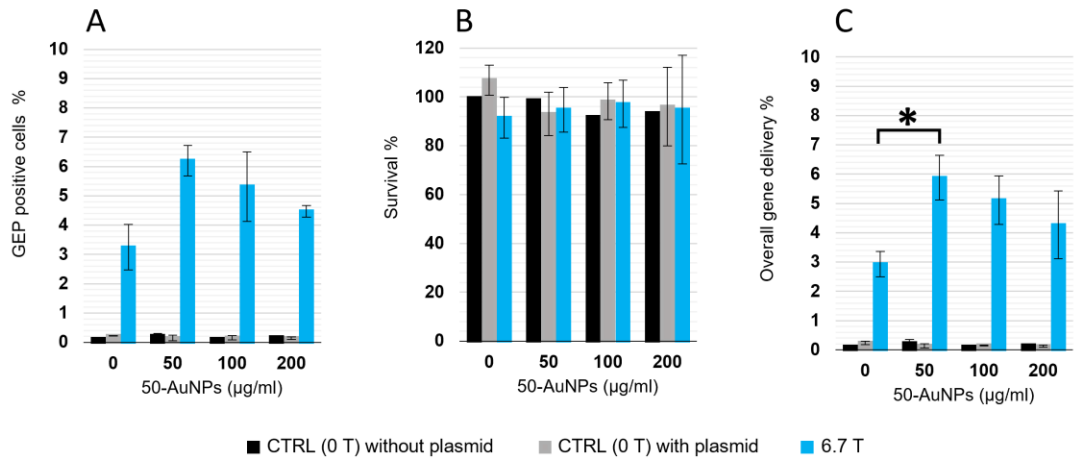

Figure 6. Gene delivery after HI-PEMF treatment on CHO cells with 50-AuNPs. A) GFP positive cells, B) survival, C) overall GET. Results are presented as a mean value and bars represent standard deviation. Asterisk (*) marks a statistically significant decrease in overall GET after HI-PEMF treatment compared to HI-PEMF treatment without NPs (0 µg/ml).

4. Discussion

The HI-PEMF induced electroporation is a non-invasive, contactless method for drugs and nucleic acids delivery into cells that may offer advantages over traditional gene electrotransfer, which relies on electroporation with direct-contact electrodes. Potentially HI-PEMF offers a technological platform to trigger painless and non-invasive electroporation, mitigating adverse effects of classical electroporation. However, since HI-PEMF is a relatively new technology with a limited number of *in vitro* studies, there remains a lack of understanding of the electromagnetic, biological, biochemical, and biophysical mechanisms underlying its effects—knowledge that is essential for further development and optimization of this treatment approach.

First, we have previously reported that the presence of gold NPs increases cell membrane permeability in HI-PEMF treatment, yet this efficacy depends on NP properties. Comparison of permeability curves performed with 5 and 20 nm gold NPs (concentrations were 10, 25, 50 µg/ml) showed that larger and more concentrated NPs resulted in better HI-PEMF treatment efficacy, i.e. higher cell membrane permeability [16]. Later we reported that HI-PEMF can be used for a successfully facilitated gene delivery [17]. However, compared to traditional electroporation (around 60%), gene delivery efficiency was considerably lower in HI-PEMF (around 3%). This was attributed to a much lower (at least 80 times lower) and non-

homogeneously distributed electric field induced by HI-PEMF. Regardless of the low numbers, this was the first successful gene transfer into cells and green fluorescent protein expression by HI-PEMF *in vitro* [17]. Based on the studies that HI-PEMF treatment can be improved by addition of NPs and successful GET with HI-PEMF treatment, combination of HI-PEMF with nanoparticles was suggested in this study .

In this work, we have studied changes in cell plasma membrane permeability when different nanoparticles were used in combination with HI-PEMF treatment. This study included six types of NPs, each differing by a single physicochemical property. This allowed us to isolate and evaluate the contribution of individual nanoparticle characteristics to HI-PEMF treatment efficacy. Comparisons between nanoparticle groups can be structured as (1) size (50-nm vs. 10-nm), (2) PEGylation (PEGylated NPs vs non-PEGylated NPs, shape (semi-spherical vs rods) and material conductivity (gold vs. silica). According to our results HI-PEMF treatment, in the presence of NPs, effects cell membrane of different cell line differently. as in this work the CHO cells were less susceptible to HI-PEMF compared to T24 cells (Figure 5). Interestingly, we could observe a NPs-specific response in the CHO cells – i.e., non-functionalized gold NPs demonstrated increase in permeabilization, while other NP types induced an opposite statistically significant effect. While smaller 10-AuNPs resulted in lower efficacy than 50-AuNPs, this difference was not statistically significant. The response of non-functionalized gold NPs is in agreement with our previous study [16]. Furthermore, comparison of PEGylated version of NPs vs non-PEGylated version of NPs (10-AuNPs-PEG vs 10-AuNPs and 50-AuNPs-PEG vs 50-AuNPs), revealed that PEGylation reduces NPs efficacy in HI-PEMF treatment. Comparison of nanoparticle shapes (semi-spherical 50-AuNPs-PEG vs rod-like AuNRs-PEG) revealed no efficacy in HI-PEMF treatment. Similar behavior was observed when different material compositions of NPs were studied (50-AuNPs vs SiO_2-NPs). In case of T24 cell line, none of the NP types involved in the study induced statistically significant improvement in cell membrane permeabilization and no differences in efficacy were detected, which suggests that NPs efficacy is cell type dependent. The cell lines used come from different species, tissue and health status (cancerous/noncancerous), which can contribute to different behavior [30].

The reason for very similar efficacy of different NP types in the HI-PEMF treatment might be in dispersing medium, where citrate buffer was replaced with cell media containing proteins.

Electroporation efficiency - probably also HI-PEMF - is strongly influenced by the composition of the electroporation buffer [31,32]. Since our HI-PEMF experiments were performed directly in complete culture media, replacing citrate buffer with cell culture medium ensured that the observed effects reflected only the contribution of nanoparticle presence, without introducing additional citrate ions into the experimental system [17,33]. Nonetheless, the citrate surface coverage of gold nanoparticles is typically reported to be between ~1–5 molecules nm^{-2} (1,2). Assuming the upper limit of 5 molecules nm^{-2}, complete desorption from the nanoparticle surface (density of gold is ~ 19.3 g/mL – relatively low specific surface area) would correspond to a maximum free citrate concentration of approximately 52 μM for 10 nm gold nanoparticles (lower citrate concentration for larger nanoparticles; at the highest tested nanoparticle concentration 200 μg/mL) in our experimental conditions. Importantly, literature indicates that biological effects of extracellular citrate—such as changes in viability, membrane permeability, or calcium homeostasis—occur only at millimolar concentrations (1–20 mM). For instance, Wu et al. [34] reported cytotoxic effects at ~5 mM citrate; Caiazza et al. [35] observed metabolic alterations at 10–20 mM; and von Schirnding et al. [36] described calcium-citrate–induced cell death only at high millimolar levels. Physiological extracellular citrate concentrations are typically around 100–150 μM [37], meaning that our estimated 52 μM—if released completely from the surface of nanoparticles—would remain well below physiologically relevant levels. However, collectively, these data strongly indicate that any potential contribution from free citrate ions would be negligible in our system, and the observed responses can be attributed to the gold nanoparticles themselves.

Furthermore, PEG-functionalized NPs provide steric stabilization, as the PEG chains (2 kDa) sterically repel NPs from each other and from the cell membrane. The PEG chains introduce steric hindrance, creating a physical barrier that prevents close interaction between the NPs and the cell membrane[38]. This steric repulsion likely limits the ability of PEG-functionalized NPs to approach or adsorb onto the membrane surface, thereby reducing their potential to locally enhance the electric field during electroporation and HI-PEMF treatment. The zeta potential values revealed that proteins from media form protein corona even in the case of PEGylated nanoparticles as the absolute values of zeta potential were decreased. This somehow shows that differences in zeta potential arising from initial functionalization (PEG vs. citrate) were effectively masked by adsorbed proteins. Therefore, consistent with this, our experiments with quasi-spherical PEG- and COOH-functionalized gold nanoparticles exhibited similar behavior across all measured endpoints.

Based on membrane permeability results, only CHO resulted in increased permeability. Therefore HI-PEMF for gene delivery was tested only on CHO cells. This was performed with nanoparticles which resulted in the highest efficacy of treatment, i.e., 50-AuNPs. As expected, gene delivery efficacy increased, from 3% to 5.9%, which is still relatively low in absolute value, yet the increase was almost 100%. Interestingly the largest percentage of GFP positive cells was at the lowest concentration of nanoparticles. The percentage of GFP positive cells dropped with an increase of nanoparticle concentration. Cell viability was unaffected even at the highest nanoparticle concentration, suggesting nanoparticles are not cytotoxic. However, the decrease in efficiency at higher nanoparticle concentrations may be due to interference with pDNA or modulation of cellular uptake processes like endocytosis, although we do not have direct evidence for this. In traditional electroporation, small molecules are believed to enter cells directly via electrophoretic transport, whereas larger molecules tend to accumulate at the membrane and are internalized via endocytosis.[4,39,40]. In contrast, our previous study indicates that HI-PEMF-mediated gene delivery occurs primarily through endocytic pathways [17]. We have also shown that HI-PEMF exposure can promote the formation of DNA–membrane complexes, which is a known prerequisite for endocytic uptake of large biomolecules [17]. We emphasize that the suggested mechanisms for the reduced efficiency at higher nanoparticle concentrations are speculative, as the exact mechanism of GET is not yet fully understood [3,41]. Testing these hypotheses directly, for example through zeta potential measurements or microscopy to observe nanoparticle–DNA–cell interactions, would require a separate study and was beyond the scope of the current work.

This study has shown the potential to enhance gene delivery efficacy using HI-PEMF treatment and NPs. However, it was observed that HI-PEMF induced effects are dependent on the cell line, nanoparticles type, concentration and therefore requires further optimization, especially for gene transfer in cancer cells.

Acknowledgement

The work has been performed within the laboratories of the Infrastructural Center of the University of Ljubljana, which is financially supported by the Slovenian Research Agency through infrastructural grant I0-0022. This work was supported by the Slovenian Research and Innovation Agency (ARIS) P2-0249, P2-0089, P3-0108, J2-3046, N2-0198, J2-60047, J2-3043, J3-3079, J7-4420. The authors acknowledge the CEMM Nanocenter (JSI, Slovenia) for

the access to electron microscopy. This work has been also partly supported by the Research Council of Lithuania, Grant. Nr. S-MIP-23-124.

Reference:

1. Ginn SL, Amaya AK, Alexander IE, et al. Gene therapy clinical trials worldwide to 2017: An update. J Gene Med 2018;20(5):1–16; doi: 10.1002/jgm.3015.

2. Broderick KE, Chan A, Lin F, et al. Optimized in vivo transfer of small interfering RNA targeting dermal tissue using in vivo surface electroporation. Mol Ther - Nucleic Acids 2012;1(2):e11; doi: 10.1038/mtna.2012.1.

3. Sachdev S, Potočnik T, Rems L, et al. Revisiting the role of pulsed electric fields in overcoming the barriers to in vivo gene electrotransfer. Bioelectrochemistry 2022;144:107994; doi: 10.1016/J.BIOELECHEM.2021.107994.

4. Rosazza C, Meglic HS, Zumbusch A, et al. Gene Electrotransfer: A Mechanistic Perspective. Curr Gene Ther 2016;16(2):98–129; doi: 10.2174/1566523216666160331130040.

5. Hernández JL, Coll T, Ciudad CJ. A highly efficient electroporation method for the transfection of endothelial cells. Angiogenesis 2004;7(3):235–241; doi: 10.1007/s10456-004-4180-8.

6. Mashel T V, Tarakanchikova Y V, Muslimov AR, et al. Biomaterials Overcoming the delivery problem for therapeutic genome editing : Current status and perspective of non-viral methods. Biomaterials 2020;258(July):120282; doi: 10.1016/j.biomaterials.2020.120282.

7. Geboers B, Scheffer HJ, Graybill PM, et al. High-Voltage Electrical Pulses in Oncology: Irreversible Electroporation, Electrochemotherapy, Gene Electrotransfer, Electrofusion, and Electroimmunotherapy. Radiology 2020;295(2):254–272; doi: 10.1148/radiol.2020192190.

8. Bradley CJ, Haines DE. Pulsed field ablation for pulmonary vein isolation in the treatment of atrial fibrillation. J Cardiovasc Electrophysiol 2020;8:2136–2147.

9. Chun K-RJ, Miklavčič D, Vlachos K, et al. State-of-the-Art Pulsed Field Ablation for Cardiac Arrhythmias : Ongoing Evolution and Future Perspective. In: Europace 2024; doi: 10.1093/europace/euae134.

10. Mahnič-Kalamiza S, Miklavcic D. The Phenomenon of Electroporation | SpringerLink. 2022. Available from: https://link.springer.com/chapter/10.1007/978-3-030-70586-2_3 [Last accessed: 5/27/2025].

11. Novickij V, Dermol J, Grainys A, et al. Membrane permeabilization of mammalian cells using bursts of high magnetic field pulses. PeerJ 2017;5(April):e3267; doi: 10.7717/peerj.3267.

12. Kranjc S, Kranjc M, Scancar J, et al. Electrochemotherapy by pulsed electromagnetic field treatment (PEMF) in mouse melanoma B16F10 in vivo. Radiol Oncol 2016;50(1):39–48; doi: 10.1515/raon-2016-0014.

13. Novickij V, Kranjc M, Staigvila G, et al. High-Pulsed Electromagnetic Field Generator for Contactless Permeabilization of Cells In Vitro. IEEE Trans Magn 2020;56(5):1–6; doi: 10.1109/TMAG.2020.2979120.

14. Chen C, Evans JA, Robinson MP, et al. Electroporation of cells using EM induction of ac fields by a magnetic stimulator. Phys Med Biol 2010;55(4):1219–1229; doi: 10.1088/0031-9155/55/4/021.

15. Kranjc Brezar S, Kranjc M, Čemažar M, et al. Electrotransfer of siRNA to Silence Enhanced Green Fluorescent Protein in Tumor Mediated by a High Intensity Pulsed Electromagnetic Field. Vaccines 2020;8(1):49; doi: 10.3390/vaccines8010049.

16. Miklavcic D, Novickij V, Kranjc M, et al. Contactless electroporation induced by high intensity pulsed electromagnetic fields via distributed nanoelectrodes. Bioelectrochemistry Amst Neth 2020;132:107440; doi: 10.1016/j.bioelechem.2019.107440.

17. Kranjc M, Dermol-Černe J, Potočnik T, et al. High-Intensity Pulsed Electromagnetic Field-Mediated Gene Electrotransfection In Vitro. Int J Mol Sci 2022;23(17):9543; doi: 10.3390/ijms23179543.

18. Goršak T, Drab M, Križaj D, et al. Magneto-mechanical actuation of barium-hexaferrite nanoplatelets for the disruption of phospholipid membranes. J Colloid Interface Sci 2020;579:508–519; doi: 10.1016/j.jcis.2020.06.079.

19. Ghorbel A, André FM, Mir LM, et al. Electrophoresis-assisted accumulation of conductive nanoparticles for the enhancement of cell electropermeabilization. Bioelectrochemistry 2021;137:107642; doi: 10.1016/j.bioelechem.2020.107642.

20. Rolong A, Prokop KJ, Davalos R V. Impact of the Use of Nanoparticles on Electric Field Distribution during Irreversible Electroporation Treatments: Can the Lesion Be Enhanced Beyond IRE Margin? In: IFMBE Proceedings 2015; pp. 793–796; doi: 10.1007/978-3-319-11128-5_197.

21. Raffa V, Riggio C, Smith MW, et al. BNNT-Mediated Irreversible Electroporation: Its Potential on Cancer Cells. Technol Cancer Res Treat 2012;11(5); doi: 10.7785/tcrt.2012.500258.

22. Zu Y, Huang S, Liao WC, et al. Gold nanoparticles enhanced electroporation for mammalian cell transfection. J Biomed Nanotechnol 2014;10(6):982–992; doi: 10.1166/jbn.2014.1797.

23. Ghorbel A, Mir LM, García-Sánchez T. Conductive nanoparticles improve cell electropermeabilization. Nanotechnology 2019;30(49):495101; doi: 10.1088/1361-6528/ab3be9.

24. Rezaee Z, Yadollahpour A, Bayati V, et al. Gold nanoparticles and electroporation impose both separate and synergistic radiosensitizing effects in HT-29 tumor cells: An in vitro study. Int J Nanomedicine 2017;12:1431–1439; doi: 10.2147/IJN.S128996.

25. Nikoobakht B, El-Sayed MA. Preparation and Growth Mechanism of Gold Nanorods (NRs) Using Seed-Mediated Growth Method. Chem Mater 2003;15(10):1957–1962; doi: 10.1021/cm020732l.

26. Liu K, Zheng Y, Lu X, et al. Biocompatible Gold Nanorods: One-Step Surface Functionalization, Highly Colloidal Stability, and Low Cytotoxicity. Langmuir 2015;31(17):4973–4980; doi: 10.1021/acs.langmuir.5b00666.

27. Ojea-Jiménez I, Bastús NG, Puntes V. Influence of the Sequence of the Reagents Addition in the Citrate-Mediated Synthesis of Gold Nanoparticles. J Phys Chem C 2011;115(32):15752–15757; doi: 10.1021/jp2017242.

28. Bastús NG, Comenge J, Puntes V. Kinetically Controlled Seeded Growth Synthesis of Citrate-Stabilized Gold Nanoparticles of up to 200 nm: Size Focusing versus Ostwald Ripening. Langmuir 2011;27(17):11098–11105; doi: 10.1021/la201938u.

29. Stöber W, Fink A, Bohn E. Controlled growth of monodisperse silica spheres in the micron size range. J Colloid Interface Sci 1968;26(1):62–69; doi: 10.1016/0021-9797(68)90272-5.

30. Hanahan D, Weinberg RA. Hallmarks of cancer: the next generation. Cell 2011;144(5):646–674; doi: 10.1016/j.cell.2011.02.013.

31. Dermol J, Pakhomova ON, Pakhomov AG, et al. Cell electrosensitization exists only in certain electroporation buffers. PLoS ONE 2016;11(7):1–19; doi: 10.1371/journal.pone.0159434.

32. Polajžer T, Dermol-Černe J, Reberšek M, et al. Cancellation effect is present in high-frequency reversible and irreversible electroporation. Bioelectrochemistry 2020;132:107442; doi: 10.1016/J.BIOELECHEM.2019.107442.

33. Polajžer T, Kranjc M, Kralj S, et al. Limited Efficacy of Nanoparticle-Assisted Electroporation for Membrane Permeabilization and Gene Electrotransfer. Pharmaceutics 2025;17(8):964; doi: 10.3390/pharmaceutics17080964.

34. Wu X, Dai H, Liu L, et al. Citrate reduced oxidative damage in stem cells by regulating cellular redox signaling pathways and represent a potential treatment for oxidative stress-induced diseases. Redox Biol 2019;21:101057; doi: 10.1016/j.redox.2018.11.015.

35. Caiazza C, D'Agostino M, Passaro F, et al. Effects of Long-Term Citrate Treatment in the PC3 Prostate Cancer Cell Line. Int J Mol Sci 2019;20(11):2613; doi: 10.3390/ijms20112613.

36. von Schirnding C, Giopanou I, Hermawan A, et al. Synergistic Combination of Calcium and Citrate in Mesoporous Nanoparticles Targets Pleural Tumors. Chem 2021;7(2):480–494; doi: 10.1016/j.chempr.2020.11.021.

37. Costello LC, Franklin RB. The implications of the hypocitricemic response to surgery and the role of liver function and hepatocyte metabolism: An important, but neglected, clinical relationship. J Liver Res Disord Ther 2018;4(3):114–119; doi: 10.15406/jlrdt.2018.04.00112.

38. Suk JS, Xu Q, Kim N, et al. PEGylation as a strategy for improving nanoparticle-based drug and gene delivery. Adv Drug Deliv Rev 2016;99(Pt A):28–51; doi: 10.1016/j.addr.2015.09.012.

39. Rosazza C, Deschout H, Buntz A, et al. Endocytosis and Endosomal Trafficking of DNA After Gene Electrotransfer In Vitro. Mol Ther Nucleic Acids 2016;5(2):e286; doi: 10.1038/mtna.2015.59.

40. Wu M, Yuan F. Membrane Binding of Plasmid DNA and Endocytic Pathways Are Involved in Electrotransfection of Mammalian Cells. PLOS ONE 2011;6(6):e20923; doi: 10.1371/journal.pone.0020923.

41. Potočnik T, Sachdev S, Polajžer T, et al. Efficient Gene Transfection by Electroporation—In Vitro and In Silico Study of Pulse Parameters. Appl Sci 2022;12(16):8237; doi: 10.3390/app12168237.